Optics Letters

Mode-resolved analysis of pump and Stokes beams in LD-pumped GRIN fiber Raman lasers

Denis S. Kharenko,[1,2,*] Mikhail D. Gervaziev,[1,2] Alexey G. Kuznetsov,[1] Evgeniy V. Podivilov,[1,2] Stefan Wabnitz,[2,3] and Sergey A. Babin[1,2]

[1]Institute of Automation and Electrometry SB RAS, 1 Ac. Koptyug Ave., Novosibirsk, Russia
[2]Novosibirsk State University, 1 Pirogova Str., Novosibirsk, Russia
[3]DIET, Sapienza University of Rome, Via Eudossiana 18, 00184 Rome, Italy
*Corresponding author: kharenko@iae.nsk.su

Received 19 November 2021; revised 21 January 2022; accepted 25 January 2022; posted 26 January 2022; published 26 February 2022

All-fiber Raman lasers have demonstrated their potential for efficient conversion of highly multimode pump beams into high-quality Stokes beams. However, the modal content of these beams has not yet been investigated. In this work, based on a mode decomposition technique, we are able to reveal the details of intermodal interactions in the different operation regimes of continuous wave multimode graded-index fiber Raman lasers. We observed that, above the laser threshold, the residual pump beam is strongly depleted in its transverse modes with principal quantum number below 10. However, the generated Stokes signal beam mainly consists of the fundamental mode, but higher-order modes are also present, albeit with exponentially decreasing population.

https://doi.org/10.1364/OL.449119

The spectral range of fiber laser emission can be significantly extended by means of the stimulated Raman scattering (SRS) effect in different operation regimes [1–4]. Most of these schemes use single-mode fibers, for which the SRS threshold is relatively low, owing to the high intensity inside the fiber core area. A new approach for multimode Raman fiber lasers (RFLs) was proposed recently: high-power multimode laser diode (LD) radiation is used as the pump, which is coupled into a multimode graded-index (GRIN) fiber, where a Raman Stokes beam with improved spatial and spectral characteristics is generated [5,6]. This method allowed for not only an extremely simple design and high efficiency of the optical to optical conversion [7], but also a significant beam quality and brightness improvement [8–10].

Specifically, it was shown that LD-pumped RFLs based on GRIN fibers permit the efficient conversion of highly multimode ($M^2 \sim 30$) continuous wave (CW) pump beams into high-quality Stokes beams with $M^2 \simeq 2$ and power $\simeq 50$ W [10]. As a result, a record pump-to-Stokes brightness enhancement (BE = 73) was demonstrated for Raman lasing at 976 nm in a multimode GRIN fiber pumped by highly multimode radiation of laser diodes at ~940 nm [11]. However, despite the nearly Gaussian shape of the generated Stokes beam, its quality parameter indicates that a noticeable contribution of high-order modes is present. Additionally, the analysis of the residual pump beam profile reveals the existence of complex mode dynamics along the gain fiber. First attempts in analysis of the transverse profile of the residual pump wave revealed that its initial parabolic shape begins to distort when the Stokes wave is generated: a dip forms in its central region [11,12]. This effect was qualitatively explained within the frame of an analytical balance model, in which the local interaction of the pump and Stokes waves is considered [11]. Since the Stokes radiation has a transverse beam size which is much smaller than that of the pump beam [due to the small transverse size of the output fiber Bragg grating (FBG) that forms the cavity], effective SRS conversion leads to a "hole burning" in the central region of the pump beam. However, the balance model does not explain quantitatively the experimentally observed significant increase, in comparison with the pump beam intensity, of the Stokes beam intensity. A more comprehensive analysis based on a numerical coupled-mode model [12] has shown that FBG spatial filtering, random mode coupling, and Kerr spatial self-cleaning all have a role in forming the output Stokes beam. However, the depleted pump radiation is only weakly sensitive to these effects. This leads to the observed pump-to-Stokes brightness enhancement in terms of integral beam profiles; however, no detailed analysis of the mode content of the residual pump and generated Stokes beams was performed.

In this Letter, we carry out this study for the first time, to the best of our knowledge, by exploiting a mode decomposition (MD) technique based on digital holography [13]. MD is an important tool in nonlinear multimode fiber (MMF) systems, since it allows for analyzing a laser beam at the output of an MMF, by providing the amplitude and phase distribution of all excited fiber modes. Our MD method [14] was earlier developed for the analysis of the Kerr beam self-cleaning of multimode sub-nanosecond pulses propagating in GRIN fibers [15]. Here we adapt the MD technique for analyzing the mode content of both pump and Stokes beams at the output of a CW GRIN-fiber RFL. As a result, we experimentally demonstrate that, above the SRS threshold, pump depletion mostly occurs among low-order degenerate mode groups. More importantly, we show that the Stokes signal has always a significant content of low-order fiber modes in addition to the fundamental mode, which explains why it cannot reach a diffraction-limited beam quality. Moreover, we obtain a new insight into the approach to the equilibrium mode

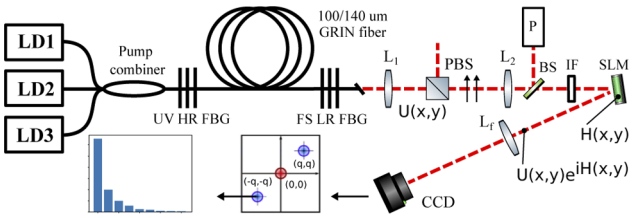

Fig. 1. Schematic of a Raman fiber laser: LDx, multimode pump laser diodes; UV HR FBG, highly reflective FBG inscribed by ultraviolet radiation; FS LR FBG, weakly reflecting FBG inscribed by femtosecond pulses; $L_{1,2}$, collimating lenses; BS, beam splitter; IF, bandpass filter; P, power meter; $U(x, y)$, output field distribution; PBS, polarization beam splitter; SLM, spatial light modulator with phase mask $H(x, y)$; L_f, Fourier lens; CCD, registration camera.

distribution in a dissipative multimode fiber system, which is different from a thermalization distribution [16], typical of the conservative case.

Our RFL is based on a multimode (MM) GRIN fiber: the generated Stokes output was earlier investigated in terms of the beam quality M^2 parameter [10] and beam profiles [11,12]. The laser setup together with the scheme of the MD system is shown in Fig. 1. The GRIN optical fiber (DrakaElite 100/140 μm, NA=0.29) has a core diameter of 100 μm and a length of 1 km. It was spooled to a standard 15-cm diameter coil. FBGs with reflectivity of ~90% and 4% and bandwidth of ~1 nm and ~0.28 nm are used as cavity mirrors [12]. An important detail here is that an output FBG with mode-dependent reflectivity is inscribed by a femtosecond laser in the central part of the fiber core: its reflectivity for the fundamental mode is 10 dB higher than that for higher-order modes (HOM). As a result, the generated Stokes beam has high quality and narrow single-peak spectrum both defined by predominant content of the fundamental mode [10–12]. An angled cleave is used to avoid back reflections from the fiber end. The RFL operates in the CW mode, and it is pumped by three fiber pigtailed MM LDs with a wavelength of ~940 nm and integral coupled pump power up to ~200 W. The CW optical power of the Stokes wave at the RFL output at 976 nm (with spectral width of 0.1–0.5 nm) is in the range from 1 W to ~50 W, with an M^2 parameter of approximately 2 at maximum power. A collimating lens and an interference filter are installed at the RFL output to send a magnified image of the near field into a spatial light modulator (SLM), while filtering out either pump or Stokes radiation, and reducing the beam powers to an acceptable level for the mode analysis with the use of SLM.

The key elements of the MD system are the SLM which selects the phase pattern corresponding to the measurement of the power fraction in each particular fiber mode, a lens (L_f) that acts as a Fourier processor, and a CCD camera for capturing the intensity distribution. A personal computer controls the SLM and processes the measured intensity distributions. A typical frame contains two first-order diffraction maxima and a zero-order spot. Any of the first-order maxima (so-called correlation answer) are useful to measure the relative mode amplitudes (shown schematically at the bottom of Fig. 1). Since the modulator requires horizontal polarization of the incident light, a polarization beam splitter (PBS) cube was installed at the input of the measurement system. Details of mathematical derivations, together with numerical calculations of the MD algorithm are given in our previous work [14].

Since the MD algorithm is based on the sequential measurement of the power carried by each individual mode, the full time for analyzing a large number of modes (approx. 80) is approximately 10 minutes. This time is relatively long, when taking into account the long-term variations of laser parameters induced by heating of pump combiner, etc. One way to reduce the measurement time is to exclude phase measurements, as they take two-thirds of all frames. Moreover, the presence of a huge amount of uncorrelated longitudinal modes does not allow us to retrieve the relative phases between transversal ones. Therefore, the overall measurement time can be significantly reduced, without compromising the MD results. In this approach, the retrieval procedure consists of obtaining the mode powers, and not the fields as in [14]. The measurement time can thus be reduced to no more than 2 minutes.

Nevertheless, it should be noted that 80 modes is a rather small number for fully characterizing the pump beam: according to previous studies [11,12], radiation occupies almost all of the GRIN fiber core. This means that, as discussed below, it was necessary to significantly increase the number of modes that were used for the MD of the pump. The next property of the MD algorithm to be considered is that it is based on progressively measuring the power fraction carried by each different mode. Thus, temporal fluctuations of the total beam power during the MD measurements directly affect the reliability of the decomposition. To mitigate this issue, the mode power values, which were measured by the camera, were corrected by continuously monitoring the total output power. In other words, at the time when the measurement of each frame took place, we also measured the corresponding total power, so that a proper normalization could be done to retrieve the relative occupation or power fraction of that particular mode. These measures allowed for accurate MD up to ~20 W of Stokes power.

By this approach, we carried out the MD of both the signal (Stokes) and the residual pump beams, which permitted us to measure the respective relative power distributions over the fiber modes for different LD pump power levels. Let us consider here two cases, below and above the SRS threshold, respectively. For understanding the general structure of the pump beam, the MD procedure was carried out below the SRS threshold up to the principal quantum number (PQN) value of 60, which corresponds to approximately 1900 fiber modes [17]. However, a qualitative analysis shows that the results of an MD for PQN>40 in our case are meaningless: for such large mode numbers, the beam is decomposed into virtually non-existing modes. This is because for such high mode numbers, their beam size fills the entire core of the fiber, so that leakage into the cladding becomes significant. For this reason, we use PQN $\leq$ 37 (total number $\leq$ 780) in presenting the MD results: as can be seen in Fig. 2, the contribution of higher-order modes rapidly declines. The validity of the mode truncation is also confirmed by the excellent agreement between the retrieved and measured beam profiles, as presented in Fig. 2.

The most interesting observation is the behavior of the mode distribution for low values of PQN (<10), below and above the SRS threshold. The results of these measurements are shown in Fig. 3. It can be seen here that, above the SRS threshold, the contribution of the first three Laguerre–Gauss (LG) modes ($LG_{0,0}$, $LG_{1,0}$, $LG_{-1,0}$) with PQN $\leq$ 1 decreases by approximately 30%. Qualitatively, we may note the flatter character of the distribution for the first 5–7 PQNs, reaching ~50% of depletion for

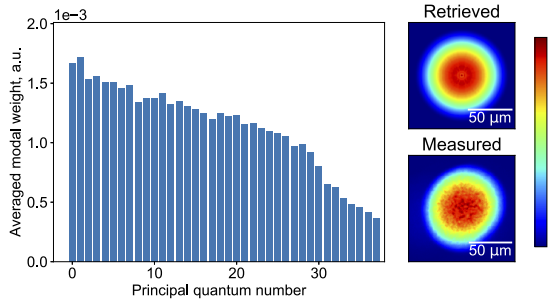

Fig. 2. (left) GRIN fiber mode power distribution for the pump beam below the Raman threshold, averaged over their degree of degeneracy; (right) reconstructed and measured residual pump beam profiles.

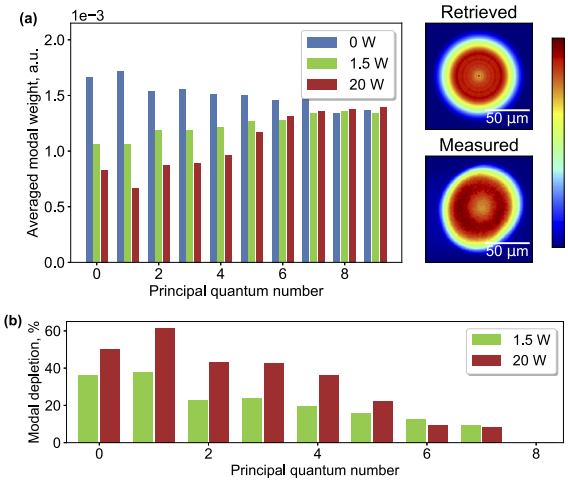

Fig. 3. (a) Power distribution over the first modes contributing to the pump beam with power under (0 W Stokes power), above (1.5 W), and well above (20 W) the SRS threshold. Modes are sorted by their PQN and averaged over their degree of degeneracy (left); the reconstructed and measured residual depleted pump beam profiles (right) are shown at the high output Stokes power. (b) Depletion percentage of the pump modes.

PQNs<5 when the Stokes power increases up to 20 W. This indicates the presence of significant interactions between the pump modes with different quantum numbers and the Stokes beam. It is noteworthy that the reconstructed and measured residual depleted pump beam profiles are in good agreement with each other.

To analyze the Stokes signal, the bandpass filter (IF) was replaced by a filter with a different center wavelength (central wavelength 975 nm, bandwidth 25 nm; Edmund Optics) in the scheme of Fig. 1. The rest of the setup remained unchanged for further experiments. The results of measuring the power distribution by performing the MD of the Stokes beam are shown in Fig. 4. Here the two cases for a low and high output Stokes power are presented together with analytical fitting curves, corresponding to an exponential (exp, dashed lines) or a Rayleigh–Jeans (RJ) law (dot–dashed lines), respectively. The dependence of the mode distribution on their PQN is much clearer than that for the residual pump beam. It can be seen that the fraction of the fundamental mode is approximately 40%, and more than 60% of the entire beam energy is concentrated in the first three modes.

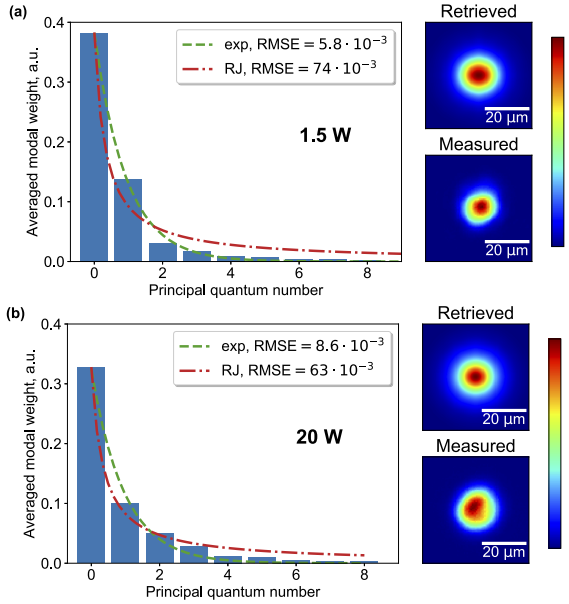

Fig. 4. Power distribution over modes contributing to the Stokes beam at (a) low (1.5 W) and (b) high (20 W) output Stokes power, sorted by their PQN and averaged over their degree of degeneracy (left); reconstructed and measured output Stokes beam profiles (right). Dashed and dot–dashed lines represent the fitting curves for exponential and RJ laws, respectively.

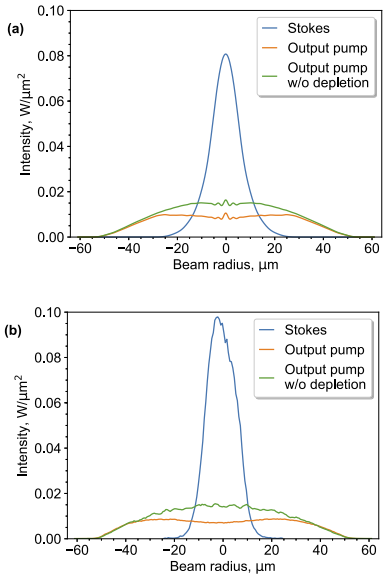

Fig. 5. Output pump and Stokes beam cross sections at 120 W input power and 20 W output Stokes power extracted from (a) decomposed and (b) measured profiles. Stokes, upper curve; Output power, middle curve; Output power w/o depletion, lower curve.

This leads to the intensity and brightness enhancement of the Stokes beam in comparison with the pump beam (Fig. 5). At the same time, the obtained data show that the excess of the previously measured parameter M^2 above 1 is due to the significant contribution of modes $LG_{1,0}$ and $LG_{-1,0}$ to the output beam of the Stokes wave.

The mode distribution in a dissipative coupled mode system such as the RFL may differ from that in the conservative case,

which is described by the RJ law, corresponding to the wave thermalization regime [16]. Here we have gain (G_k) and FBG loss (R_k) at the $(j+1)$-th round trip, resulting in the following power relation for mode k:

$$P_k^{(j+1)} = G_k R_k P_k^{(j)}. \quad (1)$$

The gain value G_k is only weakly changing with mode number k, whereas FBG filtering discriminates high-order modes against the fundamental mode by one order of magnitude, so $G_k R_k \ll G_0 R_0$. As a result, the fundamental mode is predominantly generated.

At low Stokes powers, random mode coupling dominates over nonlinear effects [12]. The presence of linear mode coupling can be taken into account in Eq. (1) as follows:

$$P_k^{(j+1)} = G_k R_k P_k^{(j)} + \sum_n |C_{k,n}|^2 [P_n^{(j)} - P_k^{(j)}]. \quad (2)$$

By supposing that the most linear coupling occurs for neighboring modes (which appears to be reasonable for a spooled fiber) so that the coupling coefficients obey $|C_{k,k+1}|^2 = C^2 \neq 0$ while other coupling coefficients tend to zero, one obtains the exponential mode distribution, which reads as

$$P_k \simeq P_0 (C^2)^k = P_0 e^{-k \ln \frac{1}{C^2}}. \quad (3)$$

By comparing the experimental mode distribution with the different analytical expressions, we can see that experiments are better described by an exponential law rather than an RJ distribution (given by dashed and dot–dashed lines in Fig. 4, respectively). This means that in a dissipative coupled mode system, we can observe a specific distribution which is mainly defined by specific gain and loss mode filtering properties and random mode coupling characteristics. However, Fig. 4 also shows that, with increasing Stokes power, a tendency towards the RJ distribution is observed, but this needs a more detailed investigation.

To summarize, we performed a quantitative analysis of the modal content of radiation from a CW fiber Raman laser made of a GRIN multimode fiber. We found that the total number of modes excited by pump radiation is approximately 780: when the SRS threshold is exceeded, the first degenerate transversal mode groups with PQN<8 are depleted by approximately 30–50% depending on power. The power distribution over modes in the Stokes wave beam is qualitatively different when compared with the pump beam. Here, approximately 40% of the entire beam energy is concentrated in the fundamental mode. On the one hand, the obtained data show that the number of modes in the generated Stokes wave is two orders of magnitude less than the number of modes which are excited by the pump wave. In addition, we proved that the deviation of the previously measured M^2 parameter of the Stokes beam from 1 is due to the significant fraction of its power (20–30%) in the $LG_{1,0}$ and $LG_{-1,0}$ modes (PQN = 1). Moreover, the nature of the mode distribution in terms of PQN turns out to be close to an exponential law. This indicates that in a dissipative mode coupling system with predominant gain and filtering of the fundamental mode, thermalization is not reached, and the mode distribution is mainly defined by random coupling between neighboring modes. However, at increasing Stokes powers, such that the Kerr effect comes into play [12], a tendency to thermalization is observed. This is due to the interplay between linear and nonlinear mode coupling, which occurs in the propagation of Stokes radiation in a 1-km-long GRIN fiber. Beyond RFLs, we believe that our results will also be of importance for the understanding of the operation of other types of multimode fiber lasers, e.g., based on spatio-temporal mode locking [18].

Funding. Russian Science Foundation (21-72-30024); Ministry of Education and Science of the Russian Federation (14.Y26.31.0017); European Research Council (740355).

Acknowledgments. The study was supported by the Russian Science Foundation (Grant No. 21-72-30024, IA&E) and by the Russian Ministry of Science and Education (Grant No. 14.Y26.31.0017, NSU), the work of S.W. was also supported by the European Research Council (grant no. 740355).

Disclosures. The authors declare no conflicts of interest.

Data availability. Data underlying the results presented in this paper are not publicly available at this time but may be obtained from the authors upon reasonable request.

REFERENCES

1. E. M. Dianov and A. M. Prokhorov, IEEE J. Sel. Top. Quantum Electron. **6**, 1022 (2000).
2. A. G. Kuznetsov, E. V. Podivilov, and S. A. Babin, Laser Phys. Lett. **12**, 035102 (2015).
3. A. G. Kuznetsov, D. S. Kharenko, E. V. Podivilov, and S. A. Babin, Opt. Express **24**, 16280 (2016).
4. D. S. Kharenko, V. D. Efremov, E. A. Evmenova, and S. A. Babin, Opt. Express **26**, 15084 (2018).
5. S. I. Kablukov, E. I. Dontsova, E. A. Zlobina, I. N. Nemov, A. A. Vlasov, and S. A. Babin, Laser Phys. Lett. **10**, 085103 (2013).
6. T. Yao, A. V. Harish, J. K. Sahu, and J. Nilsson, Appl. Sci. **5**, 1323 (2015).
7. Y. Glick, V. Fromzel, J. Zhang, N. Ter-Gabrielyan, and M. Dubinskii, Appl. Opt. **56**, B97 (2017).
8. E. A. Zlobina, S. I. Kablukov, A. A. Wolf, A. V. Dostovalov, and S. A. Babin, Opt. Lett. **42**, 9 (2017).
9. E. A. Evmenova, A. G. Kuznetsov, I. N. Nemov, A. A. Wolf, A. V. Dostovalov, S. I. Kablukov, and S. A. Babin, Sci. Rep. **8**, 17495 (2018).
10. A. G. Kuznetsov, S. I. Kablukov, A. A. Wolf, I. N. Nemov, V. A. Tyrtyshnyy, D. V. Myasnikov, and S. A. Babin, Laser Phys. Lett. **16**, 105102 (2019).
11. A. G. Kuznetsov, S. I. Kablukov, E. V. Podivilov, and S. A. Babin, OSA Continuum **4**, 1034 (2021).
12. S. A. Babin, A. G. Kuznetsov, O. S. Sidelnikov, A. A. Wolf, I. N. Nemov, S. I. Kablukov, E. V. Podivilov, M. P. Fedoruk, and S. Wabnitz, Sci. Rep. **11**, 21994 (2021).
13. D. Flamm, D. Naidoo, C. Schulze, A. Forbes, and M. Duparré, Opt. Lett. **37**, 2478 (2012).
14. M. D. Gervaziev, I. Zhdanov, D. S. Kharenko, V. A. Gonta, V. M. Volosi, E. V. Podivilov, S. A. Babin, and S. Wabnitz, Laser Phys. Lett. **18**, 015101 (2021).
15. K. Krupa, A. Tonello, B. M. Shalaby, M. Fabert, A. Barthelemy, G. Millot, S. Wabnitz, and V. Couderc, Nat. Photonics **11**, 237 (2017).
16. F. O. Wu, A. U. Hassan, and D. N. Christodoulides, Nat. Photonics **13**, 776 (2019).
17. D. S. Kharenko, M. D. Gervaziev, A. Kuznetsov, S. Wabnitz, E. V. Podivilov, and S. A. Babin, Proc. SPIE **11890**, 118901B (2021).
18. L. G. Wright, D. N. Christodoulides, and F. W. Wise, Science **358**, 94 (2017).